

NJC

New Journal of Chemistry

Accepted Manuscript

A journal for new directions in chemistry

This article can be cited before page numbers have been issued, to do this please use: S. Radisavljevic, A. Dekovic Kesic, D. Cocic, R. Puchta, L. Senft, M. Milutinovic, N. N. Milivojevi and B. Petrovic, *New J. Chem.*, 2020, DOI: 10.1039/D0NJ02037K.



This is an Accepted Manuscript, which has been through the Royal Society of Chemistry peer review process and has been accepted for publication.

Accepted Manuscripts are published online shortly after acceptance, before technical editing, formatting and proof reading. Using this free service, authors can make their results available to the community, in citable form, before we publish the edited article. We will replace this Accepted Manuscript with the edited and formatted Advance Article as soon as it is available.

You can find more information about Accepted Manuscripts in the [Information for Authors](#).

Please note that technical editing may introduce minor changes to the text and/or graphics, which may alter content. The journal's standard [Terms & Conditions](#) and the [Ethical guidelines](#) still apply. In no event shall the Royal Society of Chemistry be held responsible for any errors or omissions in this Accepted Manuscript or any consequences arising from the use of any information it contains.

1
2
3
4
5
6
7
8
9
10
11
12
13
14
15
16
17
18
19
20
21
22
23
24
25
26
27
28
29
30
31
32
33
34
35
36
37
38
39
40
41
42
43
44
45
46
47
48
49
50
51
52
53
54
55
56
57
58
59
60

Studies of the stability, nucleophilic substitution reactions, DNA/BSA interactions, cytotoxic activity, DFT and molecular docking of some tetra- and penta-coordinated gold(III) complexes

Snežana Radisavljević, ^aAna Đeković Kesić, ^bDušan Čočić, ^aRalph Puchta, ^{c,d,e}
Laura Senft, ^cMilena Milutinović, ^fNevena Milivojević^f and Biljana Petrović^{1*}

^aUniversity of Kragujevac, Faculty of Science, Department of Chemistry, Radoja Domanovića 12,
34000 Kragujevac, Serbia

^bState University of Novi Pazar, Department of Chemical-Technological Sciences,
V. Karadžića bb, 36200 Novi Pazar, Serbia

^cInorganic Chemistry, Department of Chemistry and Pharmacy, University of Erlangen-Nuremberg,
Erlangen, Germany

^dComputer Chemistry Centre, Department of Chemistry and Pharmacy, University of Erlangen-
Nuremberg, Erlangen, Germany

^eCentral Institute for Scientific Computing (ZISC), University of Erlangen-Nuremberg, Erlangen,
Germany, Germany.

^fUniversity of Kragujevac, Faculty of Science, Department of Biology, Radoja Domanovića 12, 34000
Kragujevac, Serbia

***Corresponding author:** Prof. Dr Biljana Petrović
Faculty of Science, University of Kragujevac
R. Domanovica 12, 34000 Kragujevac, Serbia
Tel: +381(0)34336223
Fax: +381(0)34335040

e-mail: biljana.petrovic@pmf.kg.ac.rs

Dedicated to our teacher, colleague and friend Prof. Dr. Dietrick K. Bretingeron the occasion of his

75th birthday.

Abstract

Two gold(III) complexes, square-planar $[\text{Au}(\text{DPP})\text{Cl}_2]^+$ (**1**) and distorted square-pyramidal $[\text{Au}(\text{DMP})\text{Cl}_3]$ (**2**) (where DMP = 2,9-dimethyl-1,10-phenanthroline and DPP = 4,7-diphenyl-1,10-phenanthroline), were studied by different experimental methods. Their stability in water and in buffer solution (25 mM HEPES, 30 mM NaCl, pH = 7.2) were investigated by UV-Vis while their redox stability is confirmed by CV. Substitution reactions between complexes **1** and **2**, and biologically relevant ligands, such as: thiourea (Tu), guanosine-5'-monophosphate (5'-GMP), glutathione (GSH) and L-methionine (L-Met), were studied by stopped-flow technique, under the *pseudo*-first order conditions as a function of ligand concentration and temperature. According to the values of the activation parameters, all studied reactions followed an associative substitution mechanism. DNA binding studies of complexes **1** and **2** were performed by UV-Vis, fluorescence spectroscopy and viscosity measurements, as like as interactions with bovine serum albumine (BSA). Density function theory (DFT) was implemented in order to analyse the wave function of the optimized structures to get better insight into the binding interactions between the inert ligands and gold(III) center. Experimental results of binding studies with DNA and BSA were simulated and compared by performing a molecular docking study. All results demonstrate the strong connection between the reactivity of the complexes toward biologically important targets and their structural and electronic characteristics. The cytotoxic activity of complexes **1** and **2** against different cell lines (MDA-MB-231, HCT-116, HaCaT) was evaluated 24 and 72 h after treatments. The results indicate reduced viability of cell lines in time- and dose- dependent manner.

Key words: gold(III), DNA, BSA, substitution, cytotoxicity

Introduction

Biological role of heavy metals (Ag, Hg, Au, Al, Pb, Cd) was usually connected with their toxicity toward living organisms.¹ But, after discovering that some platinum(II) complexes, such as cisplatin, carboplatin and oxaliplatin, show great clinical success toward different type of cancers, studies of potential application of transition metal ion complexes in pharmacy and medicine have become widely represented.^{2,3}

Gold was used in ancient Arabic and Chinese medicine, in the treatment of different diseases, like rheumatoid arthritis, malaria or HIV.^{3,4} But, during the last 20 years much interest has been focused on some gold(III) complexes, due to their stability under physiological-like conditions and *in vitro* cytotoxicity toward some human tumor cell lines.³ Particularly, coinage metals (especially Ag and Au) have been found to be a perfect candidates for this goal, because of very small damaging impact on the human body. In comparison with cisplatin, gold(III) complexes exhibit different properties (pharmaco-dynamic or kinetic), with strong cell growth inhibiting effects which makes them promising compounds for biological examination.^{5,6}

Indeed, encouraging results for *in vivo* and *in vitro* investigations were obtained after utilization of gold(III) complexes.⁷ The main problem of the biological development and usage of these compounds is poor stability in aqueous solutions. Also, gold(III) complexes are unstable under the physiological conditions due to the intracellular redox reactions with biologically relevant reducing agents.⁸⁻¹¹ This kind of reduction involves change of Au(III) to Au(I) species, responsible for further interaction with different biomolecules, DNA/BSA, proteins and enzymes. Additionally, both Au(III) and Au(I) compounds can undergo ligand exchange reactions in the presence of thiol-containing enzymes, including thioredoxin reductase. Furthermore, the change of the geometry of complexes

1
2
3 during the reduction, from square-planar to linear, is accompanied by the release of free ligands from
4 the coordination sphere of starting Au(III) complex, which can also be biologically active.¹²
5
6

7
8 However, the stability of gold(III) complexes can be improved with the appropriate choice of
9 inert ligands.¹³⁻¹⁶ Gold(III) ion generally prefer binding to the nitrogen or oxygen, because of “hard-
10 soft” Lewis theory.¹⁷ The high physiological stability and cytotoxic activity towards different human
11 tumor cell lines of some mononuclear and dinuclear gold(III) complexes was reached using the
12 nitrogen-donor ligands, such as pyridine, bipyridine, terpyridine, phenanthroline, macrocyclic ligands
13 and porphyrins.¹³⁻¹⁶ The first stable gold(III) complex with porphyrin was investigated at the beginning
14 of the 21st century and showed low IC₅₀ value (0.73-0.11 μM) on different cancer cell lines.¹⁸ Beside
15 mentioned, nitrogen-containing heterocycles and pyrimidine derivatives are important for living cell
16 metabolism and necessary for human life.^{19,20}
17
18

19 The difference of antitumor activity of platinum(II) and gold(III) complexes can be clarified
20 by observation of their mode of action. In the case of DNA, cisplatin reacts via direct interaction,²¹
21 while some Au(III) complexes show very weak interaction or modification of the double helix.
22 Gold(III) complexes have great impact on the inhibition of enzymes. Namely, due to their strong
23 binding affinity toward sulfur, different enzymes that contain sulfur, such as thioredoxin reductase,
24 glutathione reductase and cysteine protease, are potential targets for biologically active gold
25 compounds.²²⁻²⁴ Recently, we have synthesized some dinuclear and trinuclear gold(III) complexes
26 with nitrogen-donor aliphatic ligands, or gold pincer-type complexes with nitrogen-containing
27 aromatic ligands, and examined their activity against different cell lines (MDA-MB-231; HCT-116;
28 MRC-5, A549, A375, LS-174). These complexeshave shown a significant cytotoxic effect.^{9,25}
29
30
31
32
33
34
35
36
37
38
39
40
41
42
43
44
45
46
47
48
49
50

51 In an attempt to define preliminary structure–activity relationship (SAR) within the new class
52 of cytotoxic and potentially anti-tumour compounds, we have studied the properties of square-planar
53
54
55
56
57
58
59
60

[Au(DPP)Cl₂]⁺ (**1**) and distorted square-pyramidal [Au(DMP)Cl₃] (**2**) complexes (where DPP = 4,7-diphenyl-1,10-phenanthroline and DMP = 2,9-dimethyl-1,10-phenanthroline). First, we have studied the stability of complexes in water and in a buffer solution (25 mM Hepes buffer, 30 mM NaCl). Then, the kinetics and mechanism of the substitution reactions of complexes **1** and **2** with biologically relevant ligands, such as thiourea (Tu), L-methionine (L-Met), glutathione (GSH) and guanosine-5'-monophosphate (5'-GMP), were studied in 25 mM Hepes buffer and 30 mM NaCl (pH = 7.2), under the *pseudo*-first order conditions at three different temperatures. The interactions of selected complexes with representative DNA fragments, the classic target for Pt(II) complexes, were investigated as well. Furthermore, we have studied the interactions between complexes **1** and **2** and model protein bovine serum albumin (BSA), and cytotoxicity on human breast cancer cell line (MDA-MB-231), colorectal cancer cell line (HCT-116) and normal human keratinocytes cell line (HaCaT). In order to get better insight into the connection between gold(III) ion, type of the inert ligand and binding interactions with DNA and BSA, DFT calculations and simulations by molecular docking were done. All these results could throw more light on the mechanism of action and cytotoxic properties of gold(III) complexes with different geometry.

The structures of studied complexes and biologically relevant ligands are shown in Figs. 1 and

2.

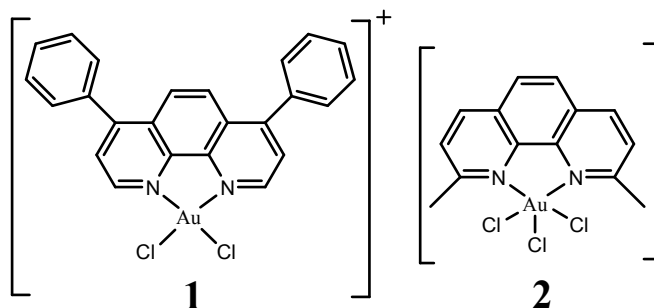


Fig. 1. The structures of studied gold(III) complexes

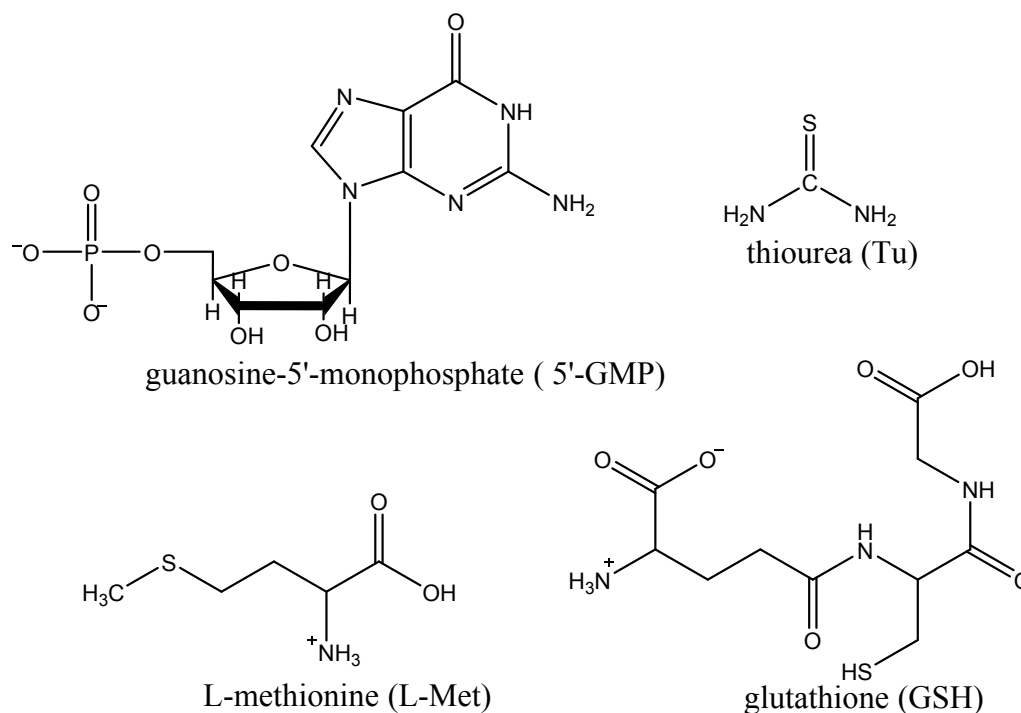


Fig. 2. The structures of studied nucleophiles

Experimental

Materials and Methods

Potassium tetrachloridoaurate(III) ($K[AuCl_4]$) and nitrogen-donor ligands (4,7-diphenyl-1,10-phenanthroline and 2,9-dimethyl-1,10-phenanthroline) were commercially available and used without purification. The nucleophiles thiourea, guanosine-5'-monophosphate, glutathione and L-methionine were obtained from Acros Organics and Aldrich. All other chemicals were of analytical reagent grade and used without further purification. Nucleophile stock solutions were prepared shortly before use by dissolving the chemicals in buffer (25 mM HEPES, 30 mM NaCl) (Sigma Aldrich). Ultrapure water was used in all experiments. Ethidium bromide (EB), calf thymus DNA (CT-DNA) and bovine serum albumin (BSA) were obtained from Sigma Chemicals Co. USA.

The stock solution of CT-DNA was prepared in buffer (25 mM Hepes, 30 mM NaCl). This solution gave a ratio of UV absorbance at 260 nm and 280 nm (A_{260}/A_{280}) of *ca.* 1.8-1.9, indicating that the DNA was sufficiently free of protein. The concentration of DNA was determined by UV absorbance at 260 nm after 1 : 20 dilution using $\epsilon = 6600 \text{ M}^{-1} \text{ cm}^{-1}$.^{26,27} Stock solution of BSA was prepared by dissolving the solid BSA in buffer (25 mM Hepes, 30 mM NaCl) at pH = 7.4. The concentration of BSA was kept fixed at 2 μM . All stock solutions were stored at 277 K and used within 5 days.

In order to obtain cyclic voltammograms, system of three electrodes was used, glassy carbon as working electrode, Ag/AgCl as reference electrode and platinum wire as a counter electrode. The surface of working electrode was polished every day or more often with alumina on a microcloth with water as the lubricant. All measurements were done at room temperature (and repeated at least three times) with scan rate 0.1 V/s, while the whole cycle was in the range +0.5 V, -0.2 V and +0.5 V. Solution of 0.1 M Et₄NBr in CH₂Cl₂ was used like supporting electrolyte. OriginPro8 and Microsoft Office Excel 2007 programs were employed with aim to analyze collected data.

Instrumentation

Chemical analyses were performed on a Varian III CHNOS Elemental Analyzer, Elemental Analysensysteme, GmbH. The UV-Vis spectra were obtained on a Perkin Elmer Lambda 35 double beam spectrophotometer, using 1.0 cm path-length quartz cuvettes (3.0 mL). Kinetic measurements were performed on an Applied Photophysics (model SX-20) stopped-flow instrument coupled to an online data acquisition system. The temperature was controlled throughout all kinetic experiments to ± 0.1 K. Infrared spectra were recorded on a Perkin Elmer 983G spectrometer. Cyclic voltammetry (CV) measurements were recorded with an Autolab PGSTAT 302N at room temperature. RF-1501 PC spectrofluorometer (Shimadzu, Japan) was used for fluorescence measurements with excitation

and emission bandwidths 10 nm. Crison EC-Meter Basic 30+ was used for measure of conductivity of freshly prepared 1.0×10^{-3} M solutions of all complexes in DMF at 25 °C. Electrospray ionization mass spectra were acquired on a Synapt G2-Si instrument (Waters).

Synthesis of the complexes

The complexes $[\text{Au}(\text{DPP})\text{Cl}_2]\text{Cl}$ (**1**) and $[\text{Au}(\text{DMP})\text{Cl}_3]$ (**2**) were prepared according to the published procedures.²⁸⁻³¹ Complex **1** was synthesized by dissolving KAuCl_4 (0.108 g, 0.28 mmol) in 5 ml of absolute methanol in the dark. A ligand was added to this solution in an equivalent ratio (0.096 g, 0.28 mmol). The mixture was stirred for 2 h at room temperature. The resulting yellow precipitate was filtered and left to dry. Elemental analysis: found: H, 1.86; C, 31.61; N, 2.86. Calc. For $\text{Au}_2\text{C}_{24}\text{H}_{16}\text{Cl}_6\text{N}_2$: H, 1.72; C, 30.70; N, 2.98 %; UV-Vis (λ_{max} , nm) 298; ESI-MS $[\text{Au}(\text{DPP})\text{Cl}_2]^+$ (m/z^+) 599; Selected IR (KBr, cm^{-1}): 3083 (w), 1626 (w), 1598 (s), 1565 (s), 1516 (m), 1425 (s), 1405 (s); Molar conductivity (λ_m , $\Omega^{-1}\text{cm}^{-1}\text{mol}^{-1}$, DMF) 79.

Complex **2** was prepared according to the similar procedure. Starting compound KAuCl_4 (0.0924 g, 0.24 mmol) was dissolved in 5 ml of absolute methanol in the dark. A ligand was added to this solution in an equivalent ratio (0.051 g, 0.24 mmol). The mixture was stirred for 2 h at room temperature and the obtained orange solution was left to evaporate at room temperature. The resulting precipitate was filtered and left to dry. Elemental analysis: found: H, 2.40; C, 32.65; N, 5.36. Calc. for $\text{AuC}_{14}\text{H}_{12}\text{Cl}_3\text{N}_2$: H, 2.36; C, 32.87; N, 5.48 %. UV-Vis (λ_{max} , nm) 270, 326; ESI-MS $[\text{Au}(\text{DMP})\text{Cl}_2]^+$ ($m/z^+ - \text{Cl}$) 475; Selected IR (KBr, cm^{-1}): 3053 (w), 2915 (w), 1591(m), 1509 (s), 1500 (s), 1428 (m); Molar conductivity (λ_m , $\Omega^{-1}\text{cm}^{-1}\text{mol}^{-1}$, DMF) < 20.

Stability of complexes 1 and 2 in aqueous solutions

The solution chemistry of complexes 1 and 2 was analyzed using UV-Vis spectrophotometry. The absorption spectra in water were recorded by diluting small amounts of freshly prepared concentrated solutions of the individual complexes in DMF. The concentration of each complex in the final sample was 1×10^{-4} M. The resulting solutions were monitored collecting the electronic spectra over 6 hours at 298 K.

Stability of complexes 1 and 2 in buffer solutions

Complexes 1 and 2 were dissolved in a few drops of DMF and then an aliquot of this solution was mixed with the medium that contain 25 mM Hepes buffer and 30 mM NaCl, to make the final concentration of complexes 5×10^{-5} M. These solutions were immediately analyzed and the spectra were collected over 6 hours at 298 K.

Kinetic measurements

Spectral changes after the mixing of equal volumes of complex and nucleophile solutions were recorded over the wavelength range 220–450 nm, to establish a suitable wavelength for kinetic measurements. The reactions were followed by stopped-flow technique, as a change of the absorbance at the working wavelength under the *pseudo*-first-order conditions (Tables S1 – S8, ESI). Nucleophile concentration was always in at least a 10-fold excess. The observed *pseudo*-first order rate constants, k_{obs} , were calculated as the average of five or six independent kinetic runs for each experimental condition. All substitution processes were studied at three different temperatures (288, 298 and 308

1
2
3 K). All calculations were performed by computational programs Microsoft Excel 2007 and
4
5 OriginPro 8.
6

7 **DNA-binding studies**

8 **Absorption spectroscopic studies**

9 UV-Vis spectroscopy was used to investigate the possible DNA-binding modes of complexes **1** and **2**
10 as well as to calculate the binding constants (K_b). The absorption titration was performed using a fixed
11 complex concentration (13.5 μM) and the increasing concentration of DNA (2.5 mM). All solutions
12 were prepared in 25 mM Hepes and 30 mM NaCl.
13

14 **Ethidium bromide (EB) displacement studies**

15 Fluorescence emission spectroscopy was carried out for the investigation of the possibility of
16 complexes **1** and **2** to displace EB from DNA-EB complex. DNA-EB was prepared 5 minutes before
17 measurements by mixing 12.5 μL of EB and 5 μL of CT-DNA in buffer solution (25 mM Hepes,
18 30 mM NaCl). The titration was performed using a fixed DNA-EB concentration (5 μM) with
19 increasing amounts of complex (2.44 μM – 23 μM). Before measurements, the solution was shaken
20 and recorded immediately. The emission was followed in the range between 550-750 nm.
21
22
23
24
25
26
27
28
29
30
31
32
33
34
35
36
37
38
39
40
41

42 **Viscosity measurements**

43 The viscosity of a CT-DNA solution was measured in the absence (η_0) and in the presence (η) of
44 increasing amounts of complexes. Digital stopwatch was used to measure a flow time. Every sample
45 was measured six times and the average flow time was calculated. The viscosity values were calculated
46 from the observed flow time of the DNA-containing solutions (t) corrected for the flow time of the
47
48
49
50
51
52
53
54
55
56
57
58
59
60

1
2
3 buffer alone (t_0), $\eta = (t-t_0)/t_0$. The data were presented as $(\eta/\eta_0)^{1/3}$ against r , where r is the ratio between
4
5 complex concentration and CT-DNA concentration.
6
7

Albumin-binding studies

8
9 The protein-binding study was performed by tryptophan fluorescence quenching experiments using
10 BSA (2 μ M) in buffer solution (25 mM Hepes, 30 mM NaCl). The quenching of the emission intensity
11 of tryptophan residues of BSA, at 361 nm and 363 nm, was monitored using complexes **1** or **2** as
12 quencher. The titration was performed using a fixed BSA concentration (2 μ M) with increasing
13 amounts of complex (0.199 μ M – 2.91 μ M). The excitation wavelength was 295 nm, while the spectra
14 were recorded in the range between 300-500 nm. The fluorescence spectra of complexes **1** and **2** in
15 buffered solutions were recorded under the same experimental conditions and no fluorescence
16 emission was recorded.
17
18
19
20
21
22
23
24
25
26
27
28
29
30
31
32

Quantum Chemical Methods

33 All quantum chemical calculations presented in this work were done applying ω B97XD functional³²
34 in combination with def2-TZVP.³³ The characterization as minima was done by computation of
35 vibrational frequencies at the same level. The GAUSSIAN suite of programs was used.³⁴ The wave-
36 function used in bonding analyses were obtained by same theory level and it analyses has been done
37 using Multiwfn program (<http://sobereva.com/wfnbbs>).³⁵ Charge decomposition analysis (CDA)
38 method³⁶ as well as QTAIM topological analysis proposed by Bader³⁷ were performed using the above
39 mention Multiwfn program package.
40
41
42
43
44
45
46
47
48
49
50
51
52
53

Molecular Docking Simulations

54
55
56
57
58
59
60

Optimized structures of investigated complexes were done as previously described in Quantum Chemical Methods of Experimental section. Structural coordinates representing a fragment of canonical B-DNA (PDB: 1BNA), DNA with an intercalation gap (PDB: 1Z3F) or BSA (PDB: 4F5S) were obtained from the Brookhaven Protein Data Bank (<http://www.rcsb.org>). In the rigid structure of DNA and BSA protein, flexible compound were docked using Molegro Virtual Docker (MVD, version 2013.6.0.1).³⁸ Water molecules, ligands, and heteroatoms were removed if present. The parameters of docking procedure were: maximum number of iterations 1500, population size 50, energy threshold 100.00, and maximum number of steps 300. Grid resolution of the binding side was 0.3 Å. The MolDock SE as a search algorithm was used with the number of runs set to 100 and the number of generated poses was 5. A maximum population of 100 and maximum number of iterations of 10 000 were used for each run. The estimation of investigated complex and DNA/BSA interactions was described by the MVD-related scoring functions: MolDock, Docking, Rerank, and Hbond.³⁷ The five best poses were retained. Molegro scores were evaluated in a relative fashion. Docked poses were visualized using CHIMERA (<http://www.cgl.ucsf.edu/chimera>) molecular graphics program.

Furthermore, the non-covalent interactions between DNA and studied complexes have been evidenced and classified using the NonCovalent Interaction (NCI) methodology.³⁹ Most notably NCI is able to discriminate between steric clashes (i.e., repulsive interactions) and dispersion π -stacking (i.e., attractive interactions with close to zero curvature). NCI analysis has been performed using Multiwfn program³⁵ on best docked poses gain by running the molecular docking simulations for two investigated complexes with two different DNA fragments (canonical and the one with intercalation gap). Previously, on this systems DFT calculation was perform with GAUSSIAN program package,³⁴ using ω B97XD functional³² in combination with def2-SVP basis set,³³ where structures of a DNA/complex gain from a molecular docking simulations were preserved but only hydrogen atoms

located on a DNA backbones were set to be optimized. Parts of DNA fragments which were not in proximity of the complexes have been removed in order to save computation time.

Cytotoxic activity and cell viability assay (MTT assay)

For cytotoxic activity, human colon (HCT-116) and breast carcinoma (MDA-MB-231) cell lines were obtained from ATCC –American Type Culture Collection, Manassas, VA, USA. Normal human keratinocytes (HaCaT) was obtained from CLS – Cell Lines Service, Eppelheim, Germany. The cells were maintained in optimum conditions and standard protocols.⁴⁰ All experiments were done with cells at 70 to 80% confluence.

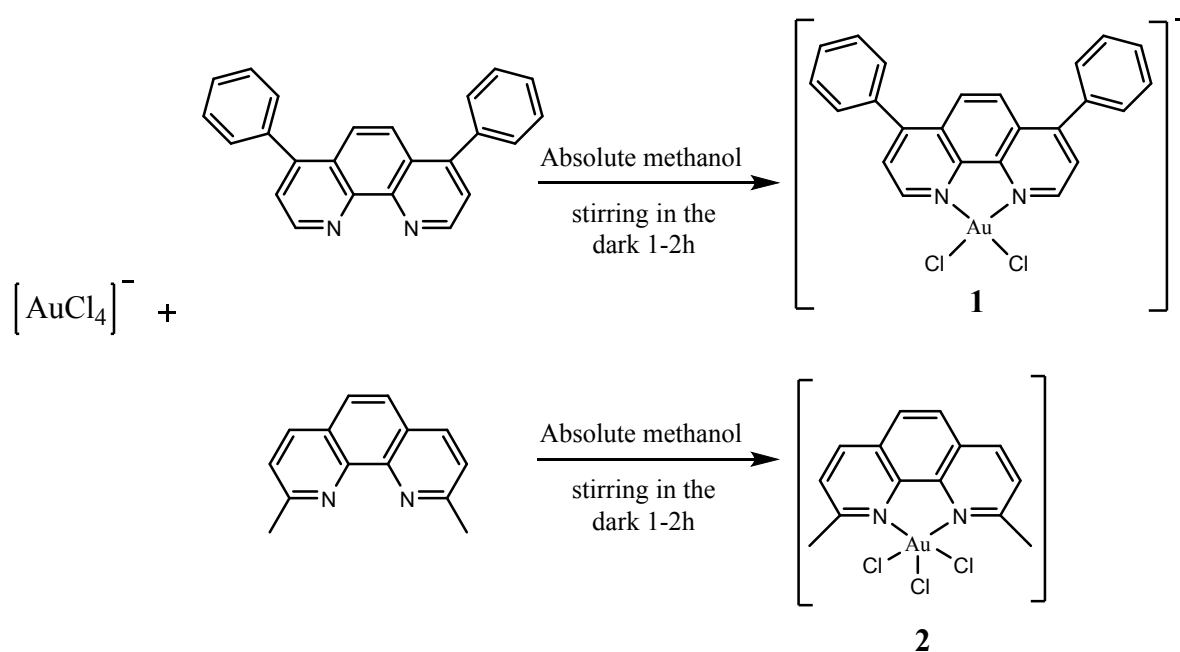
The Au(III) complexes **1** and **2** were dissolved in DMEM (Dulbecco's Modified Eagle Medium, Gibco, USA) for cell treatment, with the addition of small amount of DMSO (final concentration of DMSO was lower than 0.5 %).

Viability of MDA-231 and HCT-116 cells treated with Au(III) complexes, as well as HaCaT keratinocytes as a normal control, was evaluated by MTT assay.⁴¹ Cells were seeded in 96-well plate (10^4 cells/well), incubated 24 h and then treated by each complex in different concentrations (0.1, 1, 10, 50, 100 and 200 μ M) for 24 and 72 h. Untreated cells served as a control. At the end of the treatment period, MTT (3-[4,5-dimethylthiazol-2-yl]-2,5-diphenyltetrazolium bromide, Sigma, USA), in final concentration 5 mg/mL in PBS, was added to each well, and then incubated at 37 °C in 5% CO₂ for 2 h. The assay is based on the color reaction of mitochondrial dehydrogenase in living cells with MTT. The resulting colored crystals of formazan were dissolved in DMSO and the absorbance was measured at 550 nm. The effects on cell viability was calculated as a ratio of the absorbance of treated samples divided by the absorbance of control samples (non-treated cells), multiplied by 100 to express a percentage of viable cells.

The data are expressed as the means of two independent experiments. Biological activity is a result of two individual experiments, performed in triplicate for each dose. The magnitude of correlation between variables was done using a SPSS (Chicago, IL) statistical software package (SPSS for Windows, ver. 17, 2008). The IC_{50} values were calculated from the dose curves of cell viability by a computer program (CalcuSyn).

Results and discussion

Complexes **1** and **2** have been synthesized according to the procedure presented in Scheme 1. Their structures were confirmed by elemental analysis, spectroscopic techniques (IR, UV-Vis, ESI-MS; Figs. S1-S5, ESI) and by molar conductivity. Obtained data were in good agreement with the previously published results.²⁸⁻³¹



Scheme 1. Schematic presentation of the reactions for the synthesis of complexes **1** and **2**.

Stability of complexes **1** and **2** in aqueous solutions

The solution chemistry of complexes **1** and **2** in water was analyzed using UV-Vis spectrophotometry. Each complex was first dissolved in DMF and then diluted with water to the final concentration 1×10^{-4} . The diluted solution was analyzed over 6 hours at 298 K. Complexes have exhibited intense absorption bands in the range between 250-350 nm, assigned to N-to-gold(III) charge-transfer transitions (LMCT).^{9,42}

According to the UV-Vis spectra (Fig. S5, ESI), a decrease for complex **1** and slightly increase for complex **2** in intensity of the characteristic bands was noticed with time, without significant modifications in shape of spectra, due to hydrolysis of the gold(III)-halide bond.⁴³ The remarkable differences between these two gold complexes are observed in their time-dependent spectral changes. These changes implying that the complex **2** is a quite stable while complex **1** is less stable under the selected conditions. This can be related to the occurrence of partial hydrolysis processes or/and the formation of oligomeric species.

Stability of complexes **1** and **2** in buffer solutions

UV-Vis spectrophotometry was employed for the investigation of stability of complexes **1** and **2** at physiological pH = 7.2. The complexes were first dissolved in a few drops of DMF and then diluted with Hepes buffer (25 mM Hepes, 30 mM NaCl) to the final concentration 5×10^{-5} M. The diluted solutions were analyzed over 6 hours at 298 K. Complexes **1** and **2** exhibited intense absorption bands in the range between 250-350 nm, due to the presence of before mentioned LMCT.^{9,43}

According to the obtained UV-Vis spectra (Fig. S6, ESI), there was a very small changes in the absorption maxima after 6 hours, which can be the evidence for good stability of complexes in

1
2
3
4
5
6
7
8
9
10
11
12
13
14
15
16
17
18
19
20
21
22
23
24
25
26
27
28
29
30
31
32
33
34
35
36
37
38
39
40
41
42
43
44
45
46
47
48
49
50
51
52
53
54
55
56
57
58
59
60

buffer solution, respectively. However, the shape of spectra of these two complexes is quite different confirming the different type of coordination sphere around the gold(III) ion.²⁵

Cyclic voltammetry

The redox stability of complexes **1** and **2** was studied by cyclic voltammetry immediately after dissolution. The both cyclic voltammograms were obtained under the same conditions; concentration of complexes was 10^{-3} M, GC electrode, scan rate 0.1 V s^{-1} , $E_{\text{step}} = 0.003 \text{ V}$, $0.1 \text{ M Et}_4\text{NBr}$ in CH_2Cl_2 as the background electrolyte, Fig. 3. The cathodic peaks for both complexes were noticed, at 0.107 V and 0.121 V , respectively, while clear anodic peaks are not obtained. This can be the evidence of irreversible reduction step while the peaks in the range between $0.107 - 0.121 \text{ V}$ indicate one-electron process.⁴⁴

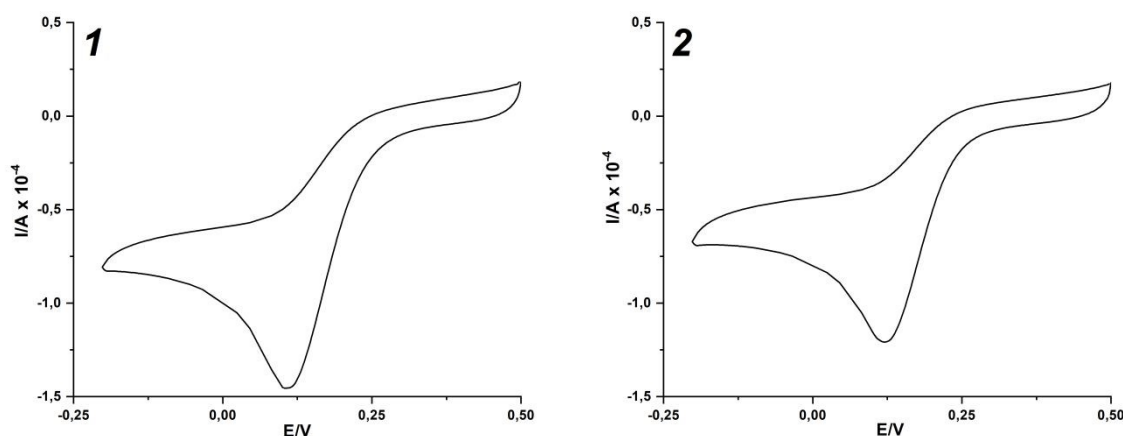


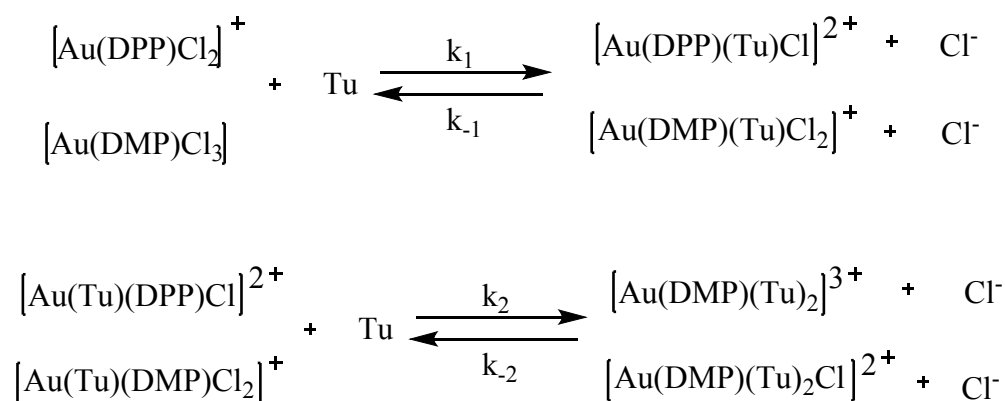
Fig. 3. Cyclic voltammograms of complexes **1** and **2** (10^{-3} M), GC electrode, scan rate 0.1 V s^{-1} , $E_{\text{step}} = 0.003 \text{ V}$, $0.1 \text{ M Et}_4\text{NBr}$ in CH_2Cl_2 as the background electrolyte.

Kinetic measurements

Stopped-flow technique was used to examine nucleophilic substitution reactions of complexes **1** and **2** with small biomolecules, such as Tu, 5'-GMP, GSH and L-Met (Fig. 2). Equal volumes of complex and nucleophile solutions were mixed directly in the stopped-flow instrument and the reactions were followed until ending. All kinetics measurements were performed under the *pseudo*-first order conditions (concentration of the nucleophile was always at least a 10-fold excess). Working wavelength for each reaction is given in Tables S1-S8, ESI.

For the square-planar metal complexes substitution reactions can occur in two parallel pathways.^{45,46} One is solvolytic pathway, resulting in a formation of a solvent-coordinated complex, followed by quick substitution of the coordinated solvent molecule by the entering nucleophile. The other pathway includes direct nucleophilic attack by the entering nucleophile. In the present study, the addition of 30 mM NaCl has the role to suppress the solvolysis, so the substitution process was happened in a reversible manner.

According to the obtained kinetic traces (Figs. S7 and S8, ESI) for each substitution process, the reactions of complexes **1** and **2** with Tu undergo through two reversible reaction steps, as suggested in Scheme 2.



Scheme 2. Proposed mechanism of substitution with Tu

The observed rate constants for the first (k_{obs1}) and the second (k_{obs2}) reaction steps are calculated by fitting the observed kinetic traces as a double exponential function and given in Tables S1 and S5, ESI. The linear dependence of k_{obs1} and k_{obs2} vs. nucleophile concentration for the reactions between complexes and Tu are described by Eqs.(1) and (2), and graphically presented on Fig. 4.

$$k_{obs1} = k_1[Tu] + k_{-1}[Cl] \quad (2)$$

$$k_{obs2} = k_2[Tu] + k_{-2}[Cl] \quad (3)$$

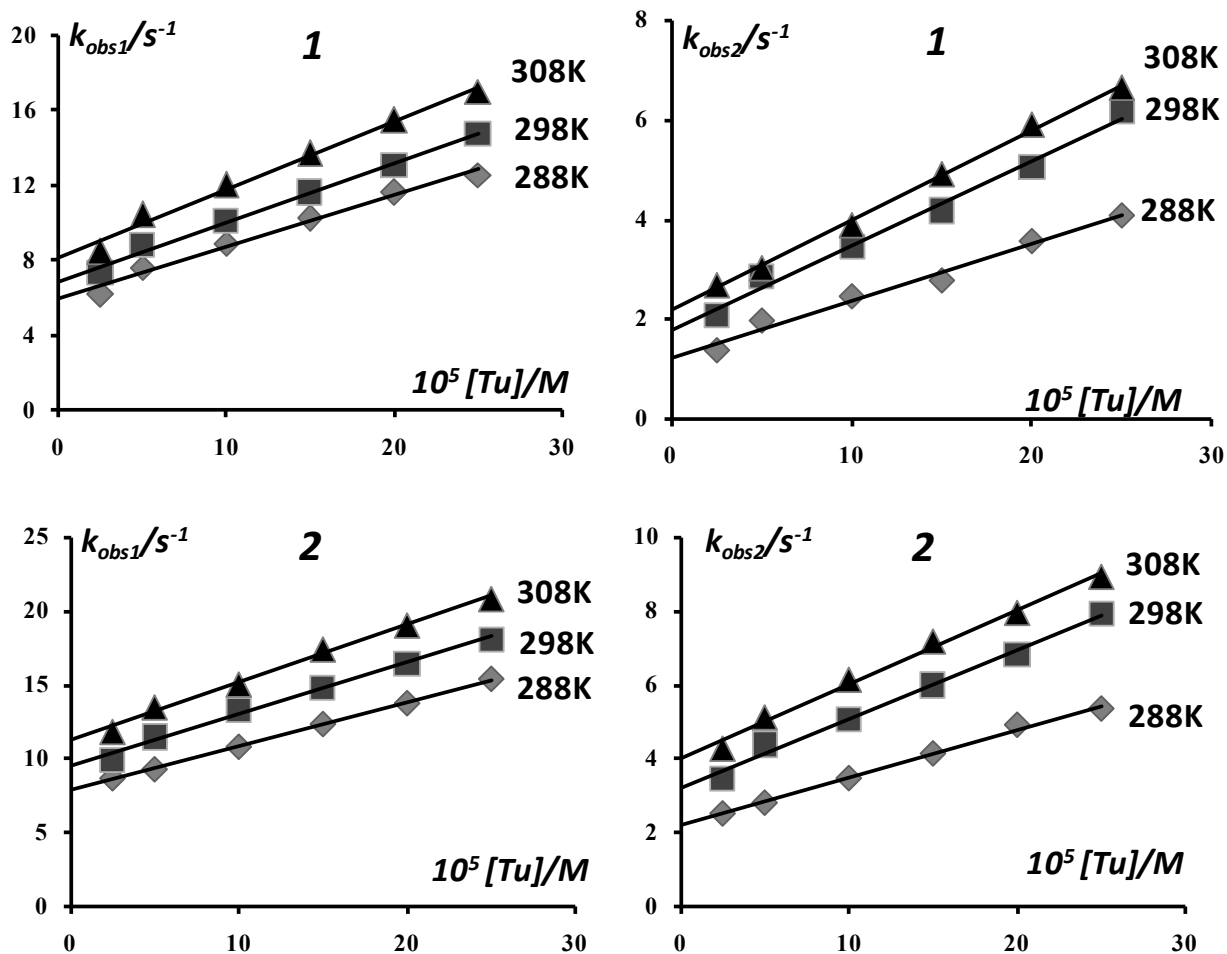
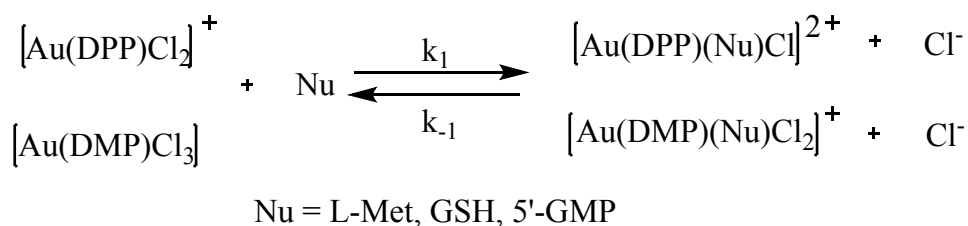


Fig. 4. Pseudo-first order rate constants for first (left) and the second (right) reaction steps of the substitution reaction between complexes **1** and **2** and Tu at pH = 7.2 (25 mM Hepes buffer, 30 mM NaCl) as a function of nucleophile concentration and temperature.

The rate constants for the direct reactions (k_1 and k_2) were calculated according to the slope of the observed lines, while from the intercept were determined the rate constants k_{-1} and k_{-2} . All values are statistically corrected and summarized in Table 1.

However, on the base of the observed kinetic traces (Fig. S7 and S8, ESI), substitution of complexes **1** and **2** with L-Met, GSH and 5'-GMP occurs as shown on Scheme 3.



Scheme 3. Proposed mechanism of substitution with L-Met, GSH and 5'-GMP

The linear dependence of k_{obs} vs. total nucleophile concentration for these reactions is described by Eq. (3) and graphically presented on Figs. S9 - S11, ESI:

$$k_{\text{obs}} = k_1[\text{Nu}] + k_{-1}[\text{Cl}] \quad (1)$$

As it was explained before, the rate constants k_1 were determined from the slope while the rate constants k_{-1} from the intercept of the observed lines. All values are given in Table 1.

1
2
3
4
5
6
7
8
9
10
11
12
13
14
15
16
17
18
19
20
21
22
23
24
25
26
27
28
29
30
31
32
33
34
35
36
37
38
39
40
41
42
43
44
45
46
47
48
49
50
51
52
53
54
55
56
57
58
59
60

Based on the values given in Table 1, all used small biomolecules are good entering ligands for the substitution reactions of investigated complexes. The reactivity of the nucleophiles decreases in order: Tu > L-Met > GSH > 5'-GMP. Higher reactivity of sulfur-donor ligands was observed compared to the nitrogen-donor ligand. Thiourea has the highest reactivity because of various ligand properties, thiolates as π -donors and thioethers as σ -donors and π -acceptors.^{43,47} Therefore, thiourea is the least sterically demanding molecule. A stronger nucleophilicity of L-Met compared with GSH can be explained due to the presence of positive inductive effect of methyl group. Additionally, for the reactions with tripeptide GSH, the transition state is additionally stabilized by the formation of intramolecular hydrogen bond which increase the nucleophilicity of sulfur atom.⁴⁸ Displacement of chloride from the starting complexes by 5'-GMP is connected with the nucleophilic attack of N7 donor atom of the purine base.⁴⁹ Taking into account that some of the used nucleophiles can be the suitable reduction agents for gold(III) complexes, during all kinetic experiments the reduction of complexes was not mentioned.

Activation parameters for all substitution processes, ΔH^\ddagger and ΔS^\ddagger , are calculated using Eyring equation. According to the negative values of ΔS^\ddagger , the activation process was strongly dominated by bond-making. Generally, the small values of ΔH^\ddagger and the negative values of ΔS^\ddagger are confirmation for an associative mode of substitution.

The difference in reactivity between complexes **1** and **2** can be ascribed to the different coordination geometry. Also, two voluminous methyl groups in the structure of complex **2** make difficult the access of the nucleophiles and formation of six-coordinated octahedral transition state through the associative mechanism of substitution.

New Journal of Chemistry Accepted Manuscript

1
2
3
4
5
6
7
8
9
10
11
12
13
14
15
16
17
18
19
20
21
22
23
24
25
26
27
28
29
30
31
32
33
34
35
36
37
38
39
40
41
42
43
44
45
46
47
48
49
50
51
52
53
54
55
56
57
58
59
60

Table 1. Rate constants and activation parameters for the substitution reactions of complexes **1** and **2** complexes with nucleophiles in 25mM Hepes buffer and 30mM NaCl (pH = 7.2).

Complex	Nucleophile	λ (nm)	T (K)	$k_1 \times 10^4$ (M ⁻¹ s ⁻¹)	k_{-1} (s ⁻¹)	ΔH_1^\ddagger (kJmol ⁻¹)	ΔS_1^\ddagger (JK ⁻¹ mol ⁻¹)
1	Tu	276	288	1.4 ± 0.2	6.0 ± 0.3	6.2 ± 0.4	-159 ± 2
			298	1.6 ± 0.1	6.9 ± 0.2		
			308	1.8 ± 0.2	8.2 ± 0.3		
2	Tu	272	288	0.99 ± 0.04	4.88 ± 0.06	6.8 ± 0.2	-159 ± 4
			298	1.17 ± 0.06	5.9 ± 0.2		
			308	1.3 ± 0.1	7.1 ± 0.2		
				$k_2 \times 10^4$ (M ⁻¹ s ⁻¹)	k_{-2} (s ⁻¹)	ΔH_2^\ddagger (kJmol ⁻¹)	ΔS_2^\ddagger (JK ⁻¹ mol ⁻¹)
1	Tu	276	288	1.10 ± 0.08	0.6 ± 0.1	10.9 ± 0.4	-144 ± 1
			298	1.49 ± 0.09	0.9 ± 0.1		
			308	1.63 ± 0.04	1.1 ± 0.1		
2	Tu	272	288	0.65 ± 0.04	0.11 ± 0.06	12.4 ± 0.6	-143 ± 2
			298	0.93 ± 0.09	0.16 ± 0.1		
			308	1.01 ± 0.09	0.20 ± 0.1		
				$k_1 \times 10^4$ (M ⁻¹ s ⁻¹)	k_{-1} (s ⁻¹)	ΔH^\ddagger (kJmol ⁻¹)	ΔS^\ddagger (JK ⁻¹ mol ⁻¹)
1	5'-GMP	255	288	0.32 ± 0.01	0.24 ± 0.02	10.0 ± 0.7	-158 ± 2
			298	0.38 ± 0.03	0.30 ± 0.05		
			308	0.46 ± 0.06	0.43 ± 0.08		
2	5'-GMP	255	288	0.20 ± 0.05	0.15 ± 0.08	10.2 ± 0.2	-161 ± 1
			298	0.24 ± 0.07	0.2 ± 0.1		
			308	0.29 ± 0.08	0.3 ± 0.1		
1	GSH	280	288	0.46 ± 0.04	0.25 ± 0.06	6.8 ± 0.2	-166 ± 4
			298	0.49 ± 0.03	0.53 ± 0.05		
			308	0.6 ± 0.6	0.9 ± 0.1		
2	GSH	294	288	0.40 ± 0.03	0.24 ± 0.05	6.0 ± 0.2	-170 ± 4
			298	0.43 ± 0.05	0.39 ± 0.07		
			308	0.51 ± 0.08	0.68 ± 0.1		
1	L-Met	295	288	0.57 ± 0.04	0.38 ± 0.07	4.7 ± 0.6	-172 ± 2
			298	0.62 ± 0.06	0.6 ± 0.1		
			308	0.7 ± 0.1	1.3 ± 0.2		
2	L-Met	294	288	0.46 ± 0.07	1.1 ± 0.1	12.1 ± 0.4	-148 ± 2
			298	0.5 ± 0.1	1.3 ± 0.1		
			308	0.7 ± 0.1	1.4 ± 0.1		

DNA binding studies

Absorption spectroscopic studies

Many metal-based anticancer agents have DNA like primary potential biological target. Accordingly, it is very important to understand the binding properties of different transition metal ion complexes. The most employed method for determination of binding mode between complexes and DNA is UV-Vis spectroscopy. It is already known that there are two possible modes of binding to DNA, covalent (replacement of the labile ligand of the complex by a nitrogen base of DNA, *e. g.*, guanine N7) or noncovalent (intercalation, electrostatic or groove binding) interactions. It is well known that absorption intensities of DNA may decrease (hypochromism) or increase (hyperchromism) with slightly increase in the absorption wavelength (bathochromism).

The absorption titration of complexes **1** and **2** in buffer (25 mM Hepes, 30 mM NaCl) was performed using a fixed complex concentration (13.5 μM) to which increments of the DNA stock solution were added (2.5 mM). The observed UV-Vis spectra of complexes **1** and **2** (200-400 nm region) in the absence and in the presence of increasing concentration of CT DNA are given in Fig. 5. The addition of certain amount of CT-DNA have caused a hyperchromism in the main absorption bands and also blue shift (298 nm \rightarrow 259 nm for complex **1**; 272 nm \rightarrow 260 nm for complex **2**), which can be the consequence of possible external binding.^{50,51} Furthermore, the appearance of a new signal in UV-Vis spectra (259 nm for complex **1**; 260 nm for complex **2**) indicates the presence of interaction between complexes and CT-DNA (Fig. 5).

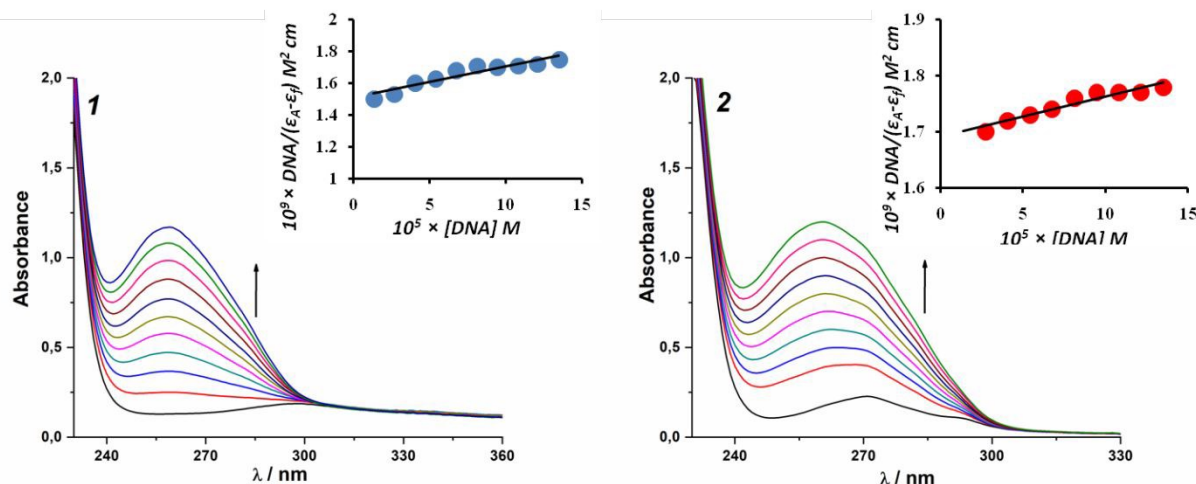


Fig. 5. Absorption spectra of complexes **1** and **2** in buffer (25 mM Hepes, 30 mM NaCl) upon addition of CT-DNA, $[\text{complex}] = 1.35 \times 10^{-5} \text{ M}$, $[\text{DNA}] = (0.134 - 1.26) \times 10^{-4} \text{ M}$. Arrow shows the absorbance changes upon increasing the DNA concentrations. Insert: Plot of $[\text{DNA}]/(\epsilon_A - \epsilon_f)$ vs. $[\text{DNA}]$

The intrinsic binding constant of complexes with CT-DNA, K_b (M^{-1}), (calculated by the Eq. S1, ESI), may be used in order to estimate binding strength. The constants are given in Table 2. Complex **1** exhibits the higher K_b value, but in comparison with K_b value for classical intercalator ethidium bromide, EB, ($K_b = (1.23 \pm 0.07) \times 10^5 \text{ M}^{-1}$),⁵² both complexes exhibit lower values of binding constants. The results obtained from UV-Vis titration experiments improves that complexes **1** and **2** can bind to CT-DNA, but the exact mode of binding cannot be described by this method.^{51,53,54}

Table 2. The DNA-binding constants (K_b) and Stern–Volmer constants (K_{sv}) for complexes **1** and **2**.

Complex	K_b (M^{-1})	K_{sv} (M^{-1})
1	$(1.29 \pm 0.02) \times 10^3$	$(4.29 \pm 0.04) \times 10^4$
2	$(4.21 \pm 0.09) \times 10^2$	$(3.19 \pm 0.03) \times 10^4$

Fluorescence quenching measurements

Complexes **1** and **2** show no fluorescence at room temperature in solution or in the presence of DNA. Furthermore, EB, a phenanthridine fluorescence dye, is an intercalator that gives a significant fluorescence emission intensity when is bound to DNA, but its displacement from EB-DNA adduct can be confirmed by decrease in fluorescence intensity.^{55,56} The changes which appear in the fluorescence emission spectra of EB-DNA are often used to describe the interaction between DNA and metal complexes. Fluorescence titration spectra of complexes **1** and **2** with EB-DNA are given in Fig. S12, ESI.

Addition of a compound, which may bind to DNA very strong (more strongly than EB), to the solution of EB-DNA results in a decrease of the DNA-induced EB fluorescence emission due to the either replacement of EB and/or electron transfer.^{54,57,58} The emission intensity at 611 nm for complex **1** and 609 nm for complex **2**, decreases with the increase of complex concentration. This may suggest that complexes **1** and **2** can replace EB from EB-DNA and interact with DNA by the intercalative mode.^{51,52,59}

The Stern-Volmer plots of EB-DNA (insert Fig. S12, ESI) confirm the fluorescence emission quenching. Stern-Volmer quenching constants (K_{sv}) are calculated from the slopes of the plots

I_0/I vs. $[Q]$ (Eq. S2, ESI) and reported in Table 2. Both complexes have showed high values of quenching constants indicating their great efficiency to replace EB and bind to DNA.

Viscosity measurements

DNA viscosity is sensitive to DNA length change. Therefore, the change of viscosity after addition of increasing amounts of compounds is often the best method to clarify the interaction mode of a compound and DNA. Usually, this is evidence for the intercalative binding mode.⁶⁰ In the case of classic intercalation, the complexes inserted between the DNA base pairs provoke an increase in the separation of base pairs at intercalation sites in order to facilitate the binding of the complexes.^{52,61,62} The magnitude of interaction is usually in accordance to the strength of the interaction, because of increasing the length of the DNA helix. Therefore, in our case DNA viscosity have increased upon addition of complexes **1** and **2**, which can be the evidence of the intercalative binding mode.^{52,61,62}

The addition of increasing amounts (up to $r = 1.0$) of complexes **1** or **2** (0-11 μM) to the DNA solution (11 μM) have resulted in an increase of relative viscosity of DNA (Fig. S13, ESI), which was more pronounced upon addition of complex **2**.

Considering that some gold(III) complexes in physiological conditions can be reduced to gold(I) and then interact with DNA¹², during these experiments the reduction was not noticed, confirming the fact that the type of inert ligands has great influence of the stability of gold(III) complexes.

Albumin binding studies

The most abundant protein in blood plasma is serum albumin (SA). Therefore, it is very important to examine the interactions of drugs with plasma proteins and especially with SA. The biological

properties of the original drug can be lost or enhance as a result of binding to these proteins. Bovine serum albumin (BSA) is the most extensively studied albumin due to its structural homology with human serum albumin (HSA).^{54,63,64} The changes and the quenching occurring in the fluorescence emission spectra of BSA upon titration with the solution of complexes may be attributed to the changes in protein conformation, subunit association, substrate binding or denaturation. The interactions of complexes **1** and **2** with BSA were studied by fluorescence spectroscopy. The observed spectra are presented in Fig. 6.

The values of the Stern-Volmer quenching constant (K_{sv}) and quenching constant (k_q) for the interaction of complexes with BSA are calculated by Stern-Volmer quenching equation (Eq. S3, ESI) and given in Table 3. The values of BSA-binding constant (K) and the number of binding sites per albumin (n) are calculated from the Scatchard equation (Eq. S4, Fig. S14, ESI). The K_{sv} and k_q values for both complexes suggest good binding propensity of the complexes.⁵³ Furthermore, the maximum of the bands was shifted from 363 nm to 393 nm and 374 nm, respectively (Fig. 6). The red shift implies the formation of gold(III)-BSA adducts, which altered the polarity of microenvironment in the vicinity of tryptophan.

Table 3. BSA constants and parameters (K_{sv} , k_q , K and n) derived for complexes **1** and **2**.

Complex	K_{sv} (M^{-1})	k_q ($M^{-1} s^{-1}$)	K (M^{-1})	n
1	$(1.11 \pm 0.02) \times 10^6$	$(1.11 \pm 0.02) \times 10^{14}$	$(3.4 \pm 0.5) \times 10^5$	0.57
2	$(2.43 \pm 0.01) \times 10^5$	$(2.43 \pm 0.01) \times 10^{13}$	$(5.0 \pm 0.3) \times 10^5$	1.41

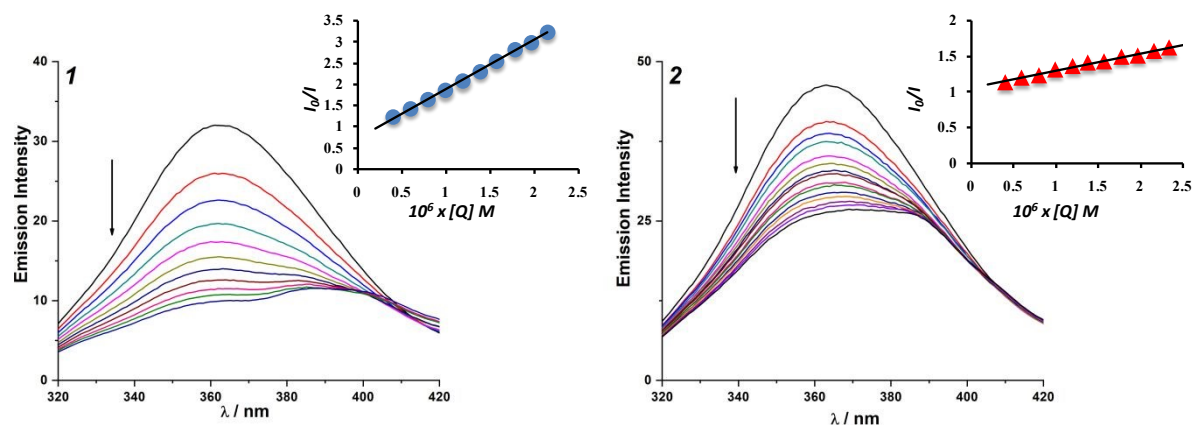


Fig. 6. Emission spectra of titration of BSA in the presence of complexes **1** and **2**. [BSA] = 2 μM ; [complex] = 0 – 2.91 μM ; λ_{ex} = 295 nm. The arrows show the intensity changes upon increasing the concentrations of complex. Insert: plots of I_0/I vs. [Q].

Both complexes have shown good quenching ability while complex **1** exhibits the stronger. Also, the k_q values for both complexes are higher than diverse kinds of quenching for biopolymer fluorescence ($10^{10} \text{ M}^{-1} \text{ s}^{-1}$) indicating the existence of a static quenching mechanism.⁶⁵

As it was mentioned before, the interactions of gold(III) complexes with serum albumin may involve the reduction of the complexes as initial step, complexes **1** and **2**, under the selected conditions, were quite stable.

Computational chemistry

The geometry-optimized structures of investigated complexes **1** and **2** are presented in Fig.7. Density function calculations at $\omega\text{B97XD/def2-TZVP}$ theory level have been performed in order to analyze the wave function of the obtained structures, focusing on the Au-N interactions in complex **2**. For

comparison, the geometry of complex $[\text{Au}(\text{phen})\text{Cl}_3]$ (**3**) (phen = 1,10-phenanthroline) (see Fig. 7) and 1,10-phenanthroline (**4**) has been optimized at the same theory level.

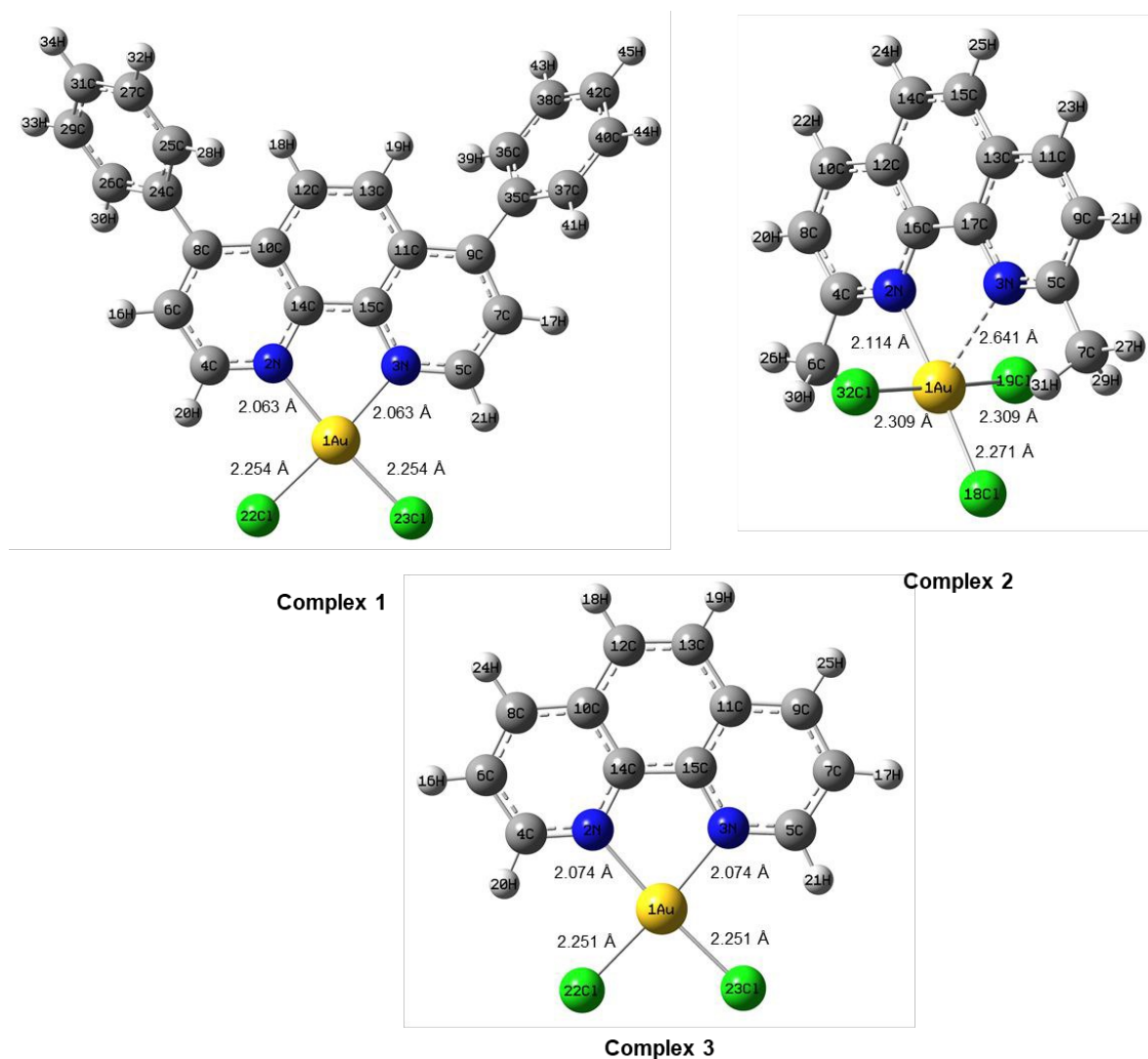


Fig. 7. Calculated ($\omega\text{B97XD}/\text{def2-TZVP}$) structures of investigated complexes with atom labeling and bond distances (\AA) around the metal center.

The calculated bond distances are in a good alignment with the previously published results of X-ray analysis.²⁷ These results together with Wiberg bond index in NAO basis and some topological properties are show in Table 4.

Table 4. Bond distances, Wiberg bond indexes in NAO basis and some topological parameters for investigated complexes **1**, **2** and **3**.

	Bonds ^a	Bond distances (Å)	WBI ^b	Topology analyses				
				BCP ^c	$\rho(r)^d$	$\nabla^2\rho(r)^e$	$H(r)^f$	$-V(r)/G(r)^g$
1	1Au-2N	2.063	0.376					
	1Au-22Cl	2.254	0.742					
2	1Au-2N	2.114	0.338	57 (3,-1)	0.1087	0.3156	-0.0359	1.32
	1Au-3N	2.641	0.103	47 (3,-1)	0.0358	0.1199	-0.0016	1.05
	1Au-18Cl	2.271	0.763					
	1Au-19Cl	2.309	0.662					
3	1Au-2N	2.074	0.365					
	1Au-22Cl	2.251	0.754					

^aSymmetrical bonds around metal center for simplicity reasons have been omitted.

^bWiberg bond index in NAO bases.

^cLabels and type for bond critical points of interest (see Fig. S15, ESI).

^dElectron density [a.u.].

^eLaplacian of electron density [a.u.].

^fEnergy density [a.u.].

^g $V(r)$ is local potential energy density and $G(r)$ represents local kinetic energy density.

According to QTAIM theory, a chemical bond is characterized by the presence of a bond critical point (BCP), corresponding to the minimum in the electron density along the bond path connecting the bonded atoms. At the BCP, the gradient of the electron density is zero, while the Laplacian $\nabla^2\rho(r)$ (Fig. S16, ESI) might either be positive or negative, positive if there is a depilation of charge at the BCP and negative if there is a local concentration of charge. Another quantitative

indicator is the energy density $H(r)$, the more negative the value, the more stabilizing (covalent) the interactions. Topological analyses of electron density according to Bader's quantum theory of atoms in molecules (QTAIM) together with the Wiberg bond index in NAO basis confirms the presence of bonding interactions between the gold atom and the nitrogen atom defined with BCP 47 (3N-1Au bond distance 2.641 Å) in DMP ligand of complex **2** (see Fig. S16, ESI, complex **2**, 3N atom label). According to the topology descriptors presented in Table 4, both Au-N bonds are characterized as predominantly ionic, which is also supported by small $\rho(r), \nabla^2\rho(r) > 0$ and $H(r) \approx 0$.

If we decompose the orbital contribution of presented BCP 47 and BCP 57, we will find that the major orbital contributions properties of BCP 57 is from LMO 36 by 71.40 % and for BCP 47 are in part from LMO 37 by 53.05 % and LMO 77 by 35.80 %. Visualization of above mentioned local molecular orbitals (LMO) is presented in Fig 8.

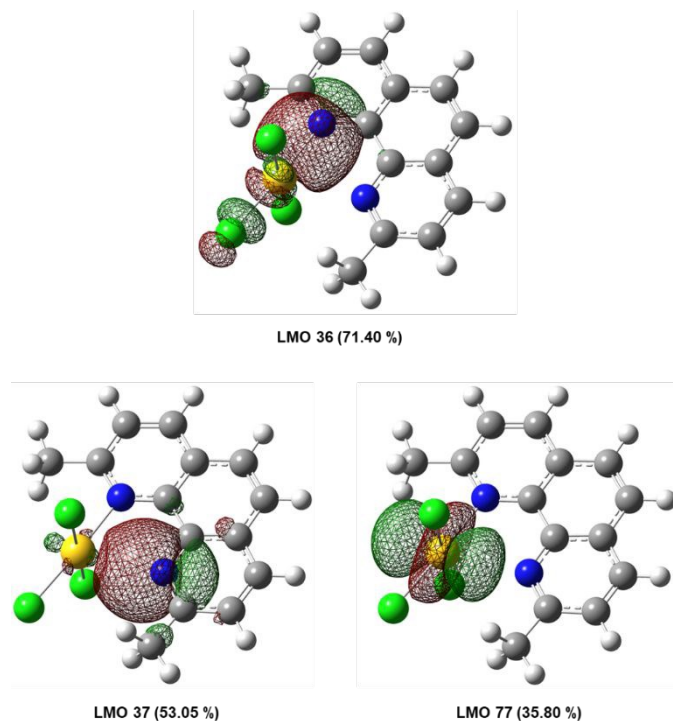


Fig. 8. Local molecular orbitals (LMO) with their contribution to the corresponding bonds.

The topological methodology of the localized orbital locator (LOL)⁶⁶ together with electron localization function (ELF) for optimized structures of **1**, **2**, **3** and **4** is shown in Fig. S17. The LOL is also a bonding descriptor and may reflect an atomic shell structure. It simply show when localized orbitals overlap, *i.e.* forming a bond, the gradient of which reaches a maximum, thereby proving a simple and recognizable pattern of a chemical bond.⁶⁷ The larger the electron localization (ELF) is in a region, the more likely the electron motion is confined within it. If electrons are completely localized, then they can be distinguished from the ones outside.⁶⁸ A large ELF value means that electrons are greatly localized, indicating that there is a covalent bond, a lone pair or inner shells of the atom involved.

Charge decomposition analysis (CDA) method is a valuable tool for analyzing the process of charge transfer between the fragments in a given complex in order to achieve the charge equilibrium. The CDA method was used to address the question of the amount of L → AuCl₂ donation and L ← AuCl₂ backdonation for complexes **1** and **3**, and L → AuCl₃ donation and L ← AuCl₃ backdonation for complex **2**. Results of CDA for mention complexes are summarized in Table 5.

Table 5. Results of CDA method for complexes **1**, **2** and **3** obtained from the ωB97XD/def2-TZVP optimized geometry.

Complex	d^a (a.u.)	b^b (a.u.)	$d-b$ (a.u.)	r^c (a.u.)
1	0.2532	0.0244	-0.2288	0.0027
2	1.0952	0.0096	-1.0855	0.0167
3	0.6319	-0.0042	-0.6361	0.0579

^a The number of electrons donated from L to AuCl₂₍₃₎

^b The number of electrons back donated from AuCl₂₍₃₎ to L

^c The number of electrons involved in repulsive polarization

From the results presented in Table 5 it can be seen that 1,10-phenanthroline based ligand of complex **1** can shift the most amount of electrons to the AuCl₂ core with the backdonation of about 10 times smaller. Complex **2** exhibit much larger donations abilities comparing to other complexes where backdonation from L in in all complexes is close to zero. During coordination between the L and AuCl₂₍₃₎, electron transfer and polarization occur, the variation of electron density can be clearly revealed by subtracting electron density of L and AuCl₂₍₃₎ in their isolated states from the whole system (complex). The purple and turquoise isosurfaces in Fig S18, ESI represent the region in which electron density is increased and decreased after L is coordinated to AuCl₂₍₃₎, respectively.

It is obvious that electron density is shifted from backside of nitrogen in L toward the metal center atom to strengthen the coordination bond. Besides, the appearance of AuCl₂₍₃₎ does perturb electron density distribution of L rings in 1,10-phenanthroline for complexes **1** and **3** remarkably. In the case of complex **2** electron density perturbation is also observed at the 3N atom (see Fig. S16, ESI) which confirms presence of bonding interactions between this nitrogen atom and the gold metal center.

Molecular docking

Molecular docking simulations is a powerful tool to test how small molecules perform interaction with biomacromolecules, in our case with DNA and BSA molecules. In the case of DNA docking two possible interactions were studied and compared, possibility of intercalation and the potential of investigated complexes to interact otherwise with the DNA fragment, e.g. minor groove. The predicted top-ranking pose for complex with the lowest energy was applied for suggesting the best possible geometry of compounds inside the DNA double helix as well as the binding inside bovine serum albumin cavity. MolDock, Docking, HBond and Rerank, scoring functions were used for the assessment of complex-DNA/BSA-binding affinity.

Our complexes were docked into DNA fragments representing either (i) canonical B-DNA (PDB 1BNA) or (ii) DNA with an intercalation gap (PDB 1Z3F). 1BNA is the crystal structure of a synthetic DNA dodecamer, while 1Z3F is the crystal structure of a 6 bp DNA fragment in complex with an intercalating anticancer drug, ellipticine. The best docked poses of complexes with DNA are displayed in Figs 9 and S19, ESI, and top-ranked poses according to used scoring functions are presented in Table 6.

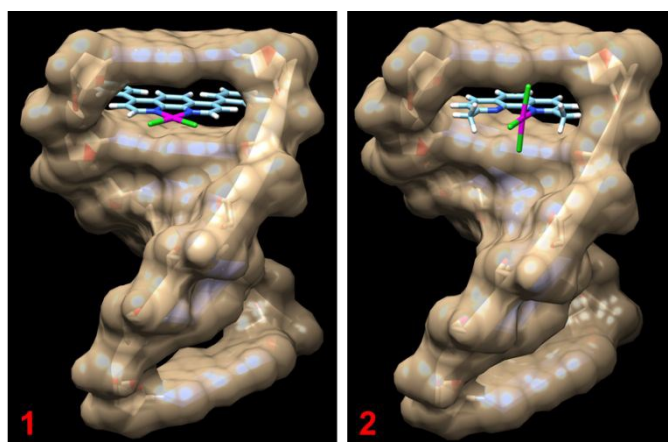


Fig. 9. Computational docking model illustrating interactions between investigated complexes and DNA with the intercalation gap.

Table 6. Score values of DNA docking with complexes **1** and **2**.

Complex	PDB ID of DNA	MolDock	Rerank	Docking
1	1Z3F – intercalation gap	-188.341	-101.457	-184.853
2		-124.483	-64.535	-121.225
1	1BNA – canonical gap	-154.715	-79.849	-151.298
2		-117.608	-60.287	-115.231

1
2
3 Values in Table 6 tell us that complex **1** has more potential for interacting stronger with DNA,
4 which can be attributed to the presents of two additional moieties on the inert
5 1,10-phenanthroline ligand and their ability for better stacking with the base pare of DNA fragments.
6 In contrast, the unique structure of complex **2** has showed to be a disadvantage in simulation process
7 of docking to the DNA fragments, which can be seen based on results presented in Table 6, and is also
8 in agreement whit the experimental results gain from absorption spectroscopic studies. Docking of the
9 investigated complexes with the 1BNA-DNA fragment was done for comparative reasons, in order to
10 compere different types of interactions to the DNA based on the MolDock scoring functions. The
11 values, as can be seen in Table 6, tell us that our complexes more prefer interactions to the DNA by
12 intercalation mode in comparison to the minor groove binding.
13
14
15
16
17
18
19
20
21
22
23
24
25
26
27
28
29
30
31
32
33
34
35
36
37
38
39
40
41
42
43
44
45
46
47
48
49
50
51
52
53
54
55
56
57
58
59
60

The docking results from the MVD program revealed that both complexes bind to the subdomain IIA (site I) of BSA protein which is consistent with the experimental data by which with the increasing amount of complexes, a fluorescence quenching was observed due to the interaction between the complexes and Trp-213 residue. Interaction results of complexes **1** and **2**, with BSA protein are illustrated in Fig. 10, while top-ranked poses according to the used scoring functions are presented in Table 7.

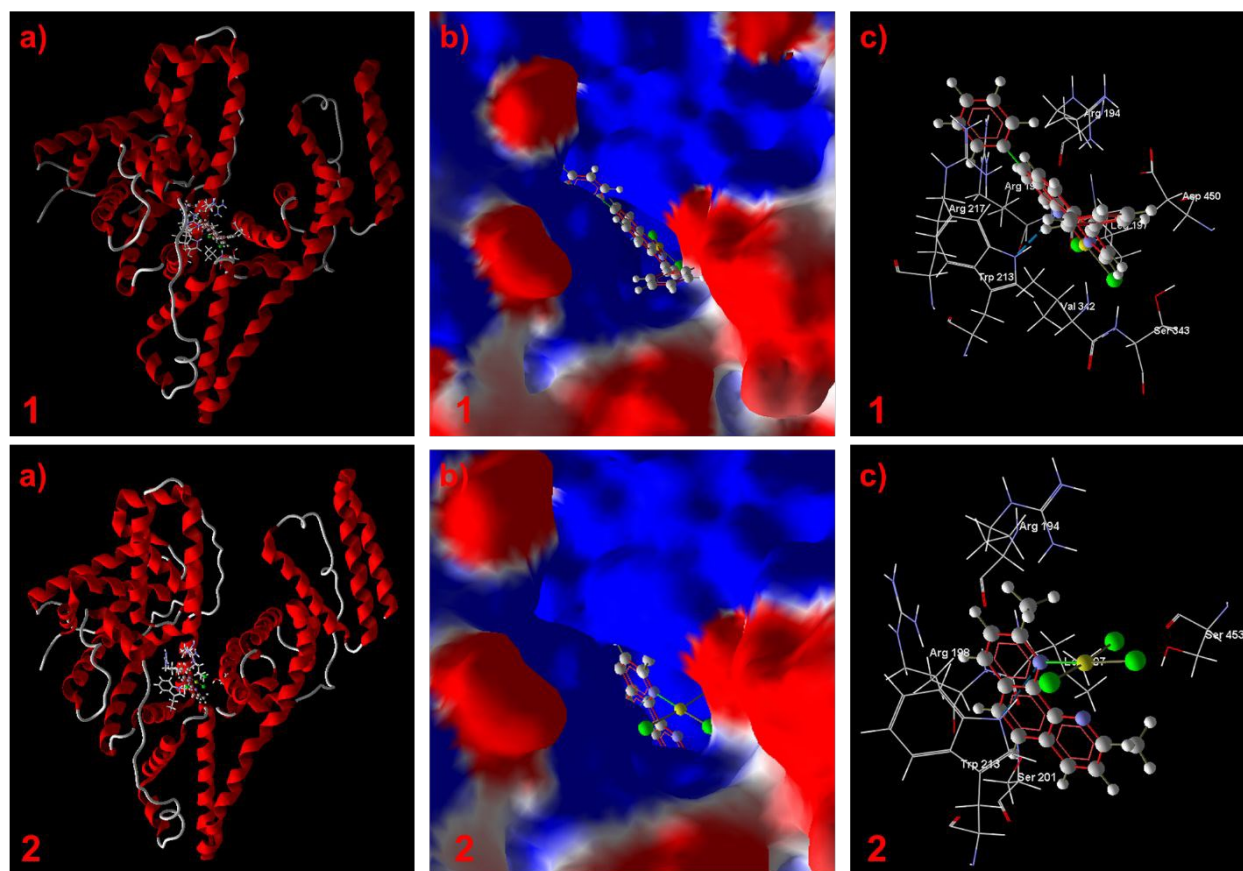


Fig. 10. Best docking poses with BSA for complexes **1** and **2** according to MolDock, Docking, HBond and Rerank scoring functions; a) molecular docking results of **1** and **2** with BSA proteins; b) complex embedded inside the active site of BSA proteins in the electrostatic view; c) binding site of investigated complexes on BSA proteins and selected amino acid residues represented by stick models (hydrogen bond are presented by blue dotted lines).

Table 7. Top-score values for complexes **1** and **2** with BSA protein.

Complex		MolDock	Rerank	HBond	Docking
1	BSA(PDB ID: 4F5S)	-109.098	-66.117	-2.349	-105.949
2		-81.501	-38.969	-1.557	-80.182

1
2
3 The displayed values tell us that the investigated complexes are very good fitted into the
4 binding pocket located at site I of BSA protein, with both steric and hydrogen bond interactions, with
5 Trp-213 residue (see c, Fig. 10.). According to the MolDock scoring functions complex **1** exhibit
6 stronger binding with the BSA protein, and this finding are also supported by the experimental results.
7

8
9 Non-covalent interaction analysis of best docked poses for investigated complexes with DNA
10 fragments is presented in Figs.11 and S20, ESI. From the color-filled RDG isosurface,³⁸ we can
11 identify different types of regions by simply examining their colors. Recalling the color scale bar,
12 interaction region marked by green circle can be identified as van der Waals interaction region. From
13 those analyses we can conclude that intercalation is most favorable type of interaction for the
14 investigated complexes, where the aromatic moieties of inert ligands inside complexes match very
15 good between the base pairs of DNA helix to further perform a π -stacking interactions as a driving
16 binding force in this particular system. Nevertheless, a larger NCI surface, corresponding to the van
17 der Waals interactions, of complex **1** compared to complex **2** is in the alignment with the results gained
18 by running the molecular docking simulations and experimentally. NCI analyses of complexes docked
19 into canonical B-DNA didn't yield any significant results compared to the intercalation gap from
20 which we concluded that the driving force in this case of interaction was only a good alignment
21 between the minor groove and a planarity of the investigated complexes.
22
23
24
25
26
27
28
29
30
31
32
33
34
35
36
37
38
39
40
41
42
43
44
45
46
47
48
49
50
51
52
53
54
55
56
57
58
59
60

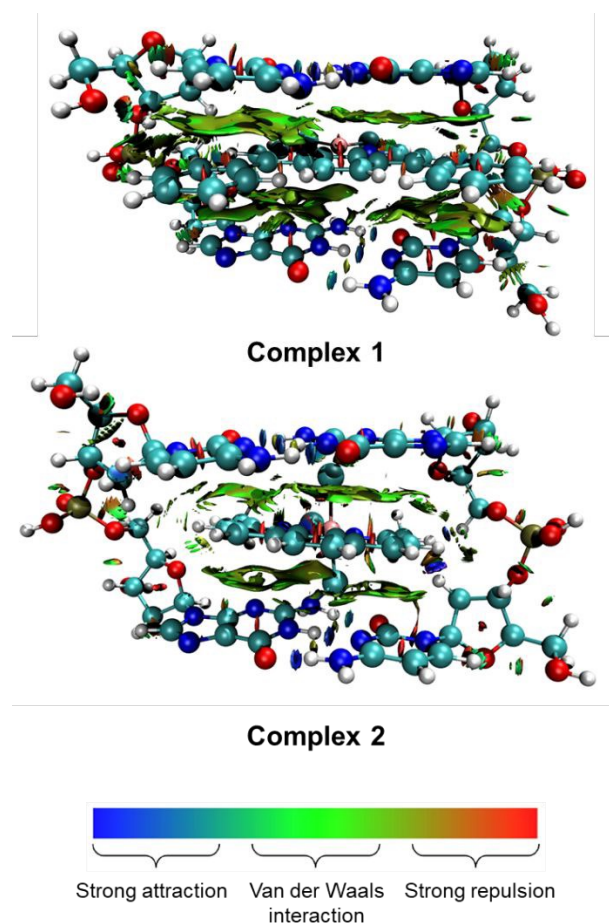


Fig. 11. NCI plot for a representative conformation of complexes **1** and **2** intercalated in the DNA double strand, surfaces represent the non-covalent interactions according to the color bar (isoval = 0.3).

Cytotoxic effects

The cytotoxic activity of complexes **1** and **2** against human breast (MDA-MB-231) and colorectal cancer (HCT-116) cell lines as well as against human normal keratinocytes (HaCaT) was evaluated 24 and 72 h after treatments by MTT cell viability assay. Both complexes significantly reduced viability of cell lines, both cancer and normal cells in time- and dose-dependent manner (Fig. S21, Tables S9-S11, ESI).

The cytotoxic activity of complexes is calculated from cell viability curves and expressed as concentration which inhibited 50% of cell growth, respectively IC_{50} value, Table 8. Both complexes show noticeable cytotoxic effects on tested cell lines according to the obtained IC_{50} values, with a slightly better effect of complex **1**. The complexes **1** and **2** expressed the highest cytotoxic effects on HCT-116 colorectal cancer cells ($IC_{50} < 25 \mu\text{M}$, Table 8). This is significant result of cytotoxicity compared to other metal complexes with different ligands currently researched.^{38,47,49,69} Also, the investigated complexes induced stronger cytotoxic activity than cisplatin on HCT-116⁷⁰ and MDA-MB-231 cells.⁷¹ However, our results indicate that studied complexes showed no selectivity toward cancer cells.

Table 8. Cytotoxic effects - IC_{50} values (μM) of complexes **1** and **2** on MDA-231, HCT-116 and HaCaT cell lines after 24 and 72 h exposure. Results are calculated upon percentages of viable cells.

Complex	IC_{50}					
	MDA-MB-231		HCT-116		HaCaT	
	24h	72h	24h	72h	24h	72h
1	28.16	0.98	3.13	0.14	10.26	1.61
2	75.02	11.75	14.57	0.01	70.58	2.40
K[AuCl₄]	101.29	150.73	>200	180.36 ^a		
cisplatin		30.8		1.6 ^b		

^a Ref. 25; ^b Ref. 72

Conclusions

In this study we put attention on establishing the relationship between reactivity and behavior in biological systems of two gold(III) complexes with similar bidentate inert ligands, derivatives of

phenanthroline. It is important to emphasize that the distorted square-pyramidal structure of complex **2** is not usual for gold(III) complexes and could be very interesting for development of similar compounds and examination of their biological behavior.

First, complexes **1** and **2** are stable in water and in a buffer solution (pH=7.2). Also, by CV measurements are confirmed their redox stability. On the base of the results of kinetic measurements, slightly higher reactivity of complex **1** is confirmed, while the reactivity of the nucleophiles follows the order: Tu > L-Met > GSH > 5'-GMP. Both complexes undergo associative substitution mechanism. The study of the interactions of complexes **1** and **2** with DNA provides multiple binding mode including covalent and intercalation interaction. Complex **1** exhibits the higher K_b value. Further, both complexes show high values of quenching constants indicating their great efficiency to replace EB and bind to DNA. According to the change of viscosity of DNA solution in the presence of complexes, better affinity for intercalation has shown complex **2**. Furthermore, relatively high binding constants toward BSA indicate a good binding affinity of both complexes, but complex **1** exhibits the stronger interaction. During all experiments, the reduction of complexes was not noticed. The values of DNA docking with complexes **1** and **2** indicate interaction with DNA by intercalation mode in comparison to the minor groove binding. The docking results from the MVD program indicate binding of complexes **1** and **2** to the subdomain IIA (site I) of BSA. The both docking results are in good agreement with experimental data. Both tested complexes reduce cell viability with cytotoxic effect on investigated cell lines, with good predisposition for potential anticancer drugs. Between them, complex **1** has shown the significant cytotoxic effects on HCT-116 colorectal cancer cells.

Conflicts of interest: There are no conflicts to declare.

Acknowledgement: The authors gratefully acknowledge financial support from the Ministry of Education and Science of the Republic of Serbia (Agreement No. 451-03-68/2020-14/200122).

References

1. B. E. Igiri, S. I. R. Okoduwa, G. O. Idoko, E. P. Akabuogu, A. O. Adeyi and I. K. Ejiogu, *J. Toxicol.*, 2018, 1-16.
2. Ž. D. Bugarčić, J. Bogojeski and R. van Eldik, *Coord Chem*, 2015, **292**, 91-106.
3. I. Ott, *Coord. Chem. Rev.*, 2009, **253**, 1670-1681.
4. G. Gu, C. Chen, Q. Wang, Z. Gao and M. Xu, *J. Appl. Spectrosc.*, 2019, **86**, 618-622.
5. V. Milacic, D. Chen, L. Ronconi, K. R. Landis-Piwowar, D. Fregona and Q. P. Dou, *Cancer Res*, 2006, **66**, 10478-10486.
6. C. Gabbiani, A. Casini and L. Messori, *Gold Bulletin*, 2007, **40**, 73-81.
7. C. Nordon, G. Boscutti, C. Gabbiani, L. Massai, N. Pettenuzzo, A. Fassina, L. Messori and D. Fregona, *Eur. J. Inorg. Chem.*, 2017, **12**, 1737-1744.
8. M. D. Đurović, Ž. D. Bugarčić and R. van Eldik, *Coord. Chem. Rev.*, 2017, **338**, 186-206.
9. S. Radisavljević, I. Bratsos, A. Scheurer, J. Korzekwa, R. Masnikosa, A. Tot, N. Gligorijević, S. Radulović and A. Rilak-Simović, *Dalton Trans.*, 2018, **47**, 13696-13713.
10. B. Đ. Glišić and M. I. Đuran, *Dalton Trans.*, 2014, **43**, 5950-5969.
11. E. R. T. Tiekink, *Inflammopharmacology*, 2008, **16**, 138-142.
12. T. Zou, C. T. Lum, C.-N. Lok, J.-J. Zhang and C.-M. Che, *Chem. Soc. Rev.*, 2015, **44**, 8786-8801.
13. B. Warzajtis, B. Đ. Glišić, M. D. Živković, S. Rajković, M. I. Đuran and U. Rychlewska, *Polyhedron*, 2015, **91**, 35-41.

- 1
2
3
4
5
6
7
8
9
10
11
12
13
14
15
16
17
18
19
20
21
22
23
24
25
26
27
28
29
30
31
32
33
34
35
36
37
38
39
40
41
42
43
44
45
46
47
48
49
50
51
52
53
54
55
56
57
58
59
60
14. K. Palanichamy, N. Sreejayan and A.C. Ontko, *J. Inorg. Biochem.*, 2012, **106**, 32-42.
 15. C. T. Lum, A. S. T. Wong, M. C. M. Lin, C. M. Che and R. W. Y. Sun, *Chem. Comm.*, 2013, **49**, 4364-4366.
 16. S. S. Al-Jaroudi, M. Monim-ul-Mehboob, M. Altaf, A. A. Al-Saadi, M. I. M. Wazeer, S. Altuwajri and A. A. Isab, *Biometals*, 2014, **27**, 1115-1136.
 17. P. Pooja, K. Ramesh, Sourabh, K. Amit, C. Pratibha and S. Rajeev, *Main Group Chem.*, 2018, **17**, 35-52.
 18. E. B. Bauer, M. A. Bernd, M. Schütz, J. Oberkofler, A. Pöthig, R. M. Reich and F. E. Kühn, *Dalton Trans*, 2019, **48**, 16615-16625.
 19. S. N. Podyachev, V. E. Semenov, V. V. Syakaev, N. E. Kashapova, S. N. Sudakova, J. K. Voronina, A. S. Mikhailov, A. D. Voloshina, V. S. Reznik and A. I. Konovalov, *RSC Advances*, 2014, **4**, 10228-10239.
 20. M. Sankarganesh, J. D. Raja, N. Revathi, R. V. Solomon and R. S. Kumar, *J. Mol. Liquids*, 2019, **294**, 111655.
 21. W. Liu and R. Gust, *Chem. Soc. Rev.*, 2013, **42**, 755-773.
 22. A. Bindoli, M. P. Rigobello, G. Scutari, C. Gabbiani, A. Casini and L. Messori, *Coord. Chem. Rev.*, 2009, **253**, 1692-1707.
 23. T. Zou, C. T. Lum, C. N. Lok, J. J. Zhang and C.M. Che, *Chem. Soc. Rev.*, 2015, **44**, 8786-8801.
 24. X. Wang and Z. Guo, *Dalton Trans.*, 2008, **12**, 1521-1532.
 25. S. Radisavljević, D. Čočić, S. Jovanović, B. Šmit, M. Petković, N. Milivojević, N. Planojević, S. Marković and B. Petrović, *J. Biol. Inorg. Chem.*, 2019, **24**, 1057-1076.

- 1
2
3
4
5
6
7
8
9
10
11
12
13
14
15
16
17
18
19
20
21
22
23
24
25
26
27
28
29
30
31
32
33
34
35
36
37
38
39
40
41
42
43
44
45
46
47
48
49
50
51
52
53
54
55
56
57
58
59
60
26. F. Dimiza, S. Fountoulaki, A. N. Papadopoulos, C. A. Kontogiorgid, V. Tangoulis, C. P. Raptopoulou, V. Psycharis, A. Terzis, D. P. Kessissoglou and G. Psomas, *Dalton Trans.*, 2011, **40**, 8555-8568.
27. F. Dimiza, F. Perdih, V. Tangoulis, I. Turel, D. P. Kessissoglou and G. Psomas, *J. Inorg. Biochem.*, 2011, **105**, 476-489.
28. N. S. Akhmadullina, A. O. Borissova, I. A. Garbuzova, V. M. Retivov, R. A. Sandu, Y. F. Kargin and O. N. Shishilov, *Z. Anorg. Allg. Chem.*, 2013, **639**, 392-397.
29. P. M. Olsen, C. Ruiz, D. Lussier, B. K. Le, N. Angel, M. Smith, C. B. Hwang, R. Khatib, J. Jenkins, K. Adams, J. Getcher, F. Tham, Z. G. Chen, E. H. Wilson and J. F. Eichler, *J. Inorg. Biochem.*, 2014, **141**, 121-131.
30. R. Ahmadi, V. Amani and H. R. Khavasi, *Acta Cryst.*, 2008, **E64**, 1156-1157.
31. W. T. Robinson and E. Sinn, *J. C. S. Dalton Trans.*, 1975, 726-731.
32. J.-D. Chai, M. Head-Gordon, *Phys. Chem. Chem. Phys.*, 2008, **10**, 6615-6620.
33. a) F. Weigend, M. Häser, H. Patzelt and R. Ahlrichs, *Chem. Phys. Lett.*, 1998, **294**, 143-152;
b) F. Weigend and R. Ahlrichs, *Phys. Chem. Chem. Phys.*, 2005, **7**, 3297-3305.
34. M. J. Frisch, G.W. Trucks, H.B. Schlegel, G.E. Scuseria, M.A. Robb, J.R. Cheeseman, G. Scalmani, V. Barone, B. Mennucci, G.A. Petersson, H. Nakatsuji, M. Caricato, X. Li, H.P. Hratchian, A.F. Izmaylov, J. Bloino, G. Zheng, J.L. Sonnenberg, M. Hada, M. Ehara, K. Toyota, R. Fukuda, J. Hasegawa, M. Ishida, T. Nakajima, Y. Honda, O. Kitao, H. Nakai, T. Vreven, J.A. Montgomery, Jr., J.E. Peralta, F. Ogliaro, M. Bearpark, J.J. Heyd, E. Brothers, K.N. Kudin, V.N. Staroverov, T. Keith, R. Kobayashi, J. Normand, K. Raghavachari, A. Rendell, J.C. Burant, S.S. Iyengar, J. Tomasi, M. Cossi, N. Rega, J.M. Millam, M. Klene, J.E. Knox, J.B. Cross, V. Bakken, C. Adamo, J. Jaramillo, R. Gomperts, R.E. Stratmann, O.

- 1
2
3 Yazyev, A.J. Austin, R. Cammi, C. Pomelli, J.W. Ochterski, R.L. Martin, K. Morokuma, V.G.
4 Zakrzewski, G.A. Voth, P. Salvador, J.J. Dannenberg, S. Dapprich, A.D. Daniels, O. Farkas,
5 J.B. Foresman, J.V. Ortiz, J. Cioslowski and D.J. Fox, GAUSSIAN 09 (Revision C.01),
6 Gaussian, Inc., Wallingford, CT (2010).
7
8
9
10
11
12
13
14
15
16
17
18
19
20
21
22
23
24
25
26
27
28
29
30
31
32
33
34
35
36
37
38
39
40
41
42
43
44
45
46
47
48
49
50
51
52
53
54
55
56
57
58
59
60
35. T. Lu and F. Chen, *J. Comput. Chem.*, 2012, **33**, 580-592.
36. a) S. Dapprich and G. Frenking, *J. Phys. Chem.*, 1995, **99**, 9352–9362; b) X. Meng and L. Tian, *Adv. Phys. Chem.*, 2015, **4**, 111-124.
37. a) R. F. W. Bader, *Atoms in Molecules. A Quantum Theory*, Clarendon Press, Oxford, U.K., 1994; b) P. L. A. Popelier, *Atoms in Molecules. An Introduction*, Prentice Hall, Harlow, 2000.
38. R. Thomsen and M. H. Christensen, *J. Med. Chem.*, 2006, **49**, 3315–3321.
39. E. R. Johnson, S. Keinan, P. Mori-Sánchez, J. Contreras-García, A. J. Cohen and W. Yang, *J. Am. Chem. Soc.* 2010, **132**, 6498-6506.
40. M. Milutinović, M. Stanković, D. Cvetković, V. Maksimović, B. Šmit, R. Pavlović and S. Marković, *J. Food Biochem.*, 2015, **39**, 238-250.
41. T. Mosmann, *J. Immunol. Meth.*, 1983, **65**, 55-63.
42. L. Ronconi, C. Marzano, P. Zanello, M. Corsini, G. Miolo, C. Maccà, A. Trevisan and D. Fregona, *J. Med. Chem.*, 2006, **49**, 1648-1657.
43. M. T. Ashby, *Comments Inorg. Chem.*, 1990, **10**, 297-313.
44. N. Pantelić, D. M. Stanković, B. B. Zmejkovski, G. N. Kaluđerović and T. J. Sabo, *Int. J. Electrochem. Sci.*, 2016, **11**, 1162-1171.
45. M. L. Tobe and J. Burgess, *Inorganic Reaction Mechanisms*, Addison Wesley Longman Inc, Essex, 1999, 70-112.
46. H. S. Leif, A. G. Sykes (Ed.), *Adv. Inorg. Bioinorg. Mech.*, Academic Press, 1986, 137-183.

- 1
2
3
4
5
6
7
8
9
10
11
12
13
14
15
16
17
18
19
20
21
22
23
24
25
26
27
28
29
30
31
32
33
34
35
36
37
38
39
40
41
42
43
44
45
46
47
48
49
50
51
52
53
54
55
56
57
58
59
60
47. S. G. Murray and F. R. Hartley, *Chem. Rev.*, 1981, **81**, 365-414.
48. A. Hofmann, D. Jaganyi, O. Q. Munro, G. Liehr and R. van Eldik, *Inorg. Chem.*, 2003, **42**, 1688-1700.
49. P. J. Sadler and R. E. Sue, *Met.-Based Drugs*, 1994, **1**, 107-144.
50. K. C. Skyrianou, F. Perdih, I. Turel, D. P. Kessissoglou and G. Psomas, *J. Inorg. Biochem.* 2010, **104**, 740-749.
51. A. Tarushi, C. P. Raptopoulou, V. Psycharis, A. Terzis, G. Psomas and D. P. Kessissoglou, *Bioorg. Med. Chem.*, 2010, **18**, 2678-2685.
52. A. Tarushi, K. Lafazanis, J. Kljun, I. Turel, A. A. Pantazaki, G. Psomas and D. P. Kessissoglou, *J. Inorg. Biochem.*, 2013, **121**, 53-65.
53. A. A. R. Despaigne, J. G. D. Silva, P. R. D. Costa, R. G. D. Santos and H. Beraldo, *Molecules*, 2014, **19**, 17202-17220.
54. A. Tarushi, E. Potatoglou, J. Kljun, I. Turen, G. Psomas and D. P. Kessissoglou, *Dalton Trans.*, 2011, **40**, 9461-9473.
55. C. V. Kumar, J. K. Barton and N. J. Turro, *J. Am. Chem. Soc.*, 1985, **107**, 5518-5523.
56. W. D. Wilson, L. Ratmeyer, M. Zhao, L. Strekowski and D. Boykin, *Biochem.*, 1993, **32**, 4098-4104.
57. S. Shar, M. Nethaji and A. R. Chakravarty, *J. Inorg. Biochem.*, 2005, **99**, 805-812.
58. R. F. Pasternack, M. Caccam, B. Keogh, T. A. Stephenson, A. P. Williams and E. J. Gibbs, *J. Am. Chem. Soc.*, 1991, **113**, 6835-6840.
59. F. Dimiza, S. Fountoulaki, A. N. Papadopoulos, C. A. Kontogiorgis, V. Tangoulis, C. P. Raptopoulou, V. Psycharis, A. Terzis, D. P. Kessissoglou and G. Psomas, *Dalton Trans*, 2011, **40**, 8555-8568.

- 1
2
3 60. D.-D. Li, J.-L. Tian, W. Gu, X. Liu and S.-P. Yan, *J. Inorg. Biochem.*, 2010, **104**, 171-179.
- 4
5
6 61. J. L. García-Giménez, M. Gonzáles-Álvarez, M. Liu-Gonzáles, B. Macías, J. Borrás and G.
7
8 Alzuet, *J. Inorg. Biochem.*, 2009, **103**, 923-934.
- 9
10 62. J. Liu, H. Zhang, C. Chen, H. Deng, T. Lu and L. Ji, *Dalton Trans.*, 2003, 114-119.
- 11
12 63. C. Tan, J. Liu, H. Li, W. Zheng, S. Shi, L. Chen and L. Ji, *J. Inorg. Biochem.*, 2008, **102**, 347-
13
14 358.
- 15
16 64. J. R. Lakowicz, *Principles of Fluorescence Spectroscopy*, 3rd ed., Springer, New York, 2006.
- 17
18 65. Y.-Q. Wang, H.-M. Zhang, G.-C. Zhang, W.-H. Tao and S.-H. Tang, *J. Lumin.*, 2007, **126**,
19
20 211-218.
- 21
22 66. H. L. Schmider and A. D. Becke, *J. Mol. Struct.: THEOCHEM*, 2000, **527**, 51–61.
- 23
24 67. H. L. Schmider and A. D. Becke, *J. Chem. Phys.*, 2002, **116**, 3184–3193.
- 25
26 68. T. Lu and F.-W. Chen, *Acta Phys.-Chim. Sin.*, 2011, **27**, 2786-2792.
- 27
28 69. V. P. Petrović, M. N. Živanović, D. Simijonović, J. Đorović, Z. D. Petrović and S. D.
29
30 Marković, *RSC Advances*, 2015, **5**, 86274-86281.
- 31
32 70. M. M. U. Mazumder, A. Sukul, S. K. Saha, A. A. Chowdhury and Y. Mamun, *Alexandria J.*
33
34 *Med.*, 2018, **54**, 23-26.
- 35
36 71. K. Bielawski, A. Bielawska, T. Slodownik, B. Poplawska and U. Bolkun-Skórnicka, *Acta Pol.*
37
38 *Pharm.*, 2008, **65**, 135-140.
- 39
40 72. M. M. Zarić, P. P. Čanović, M. S. Pirković, S. M. Knežević, R. S. Živković Zarić, B.
41
42 PopovskaJovičić, N. Hamzagić, B. Simović Marković, N. Marković and A. Rilak Simović,
43
44 *Vojno sanitetski pregled*, 2020, doi:10.2298/VSP190507002Z.
- 45
46
47
48
49
50
51
52
53
54
55
56
57
58
59
60

Graphical abstract

This paper cover the study of the stability in water and in buffer solution (pH = 7.2), nucleophilic substitution reactions with Tu, 5'-GMP, GSH and L-Met), DNA/BSA interactions, cytotoxic activity, DFT and molecular docking of tetra- and penta-coordinated gold(III) complexes with phenanthroline derivatives as inert ligands.

